Improvement of algorithms for digital real-time n-γ discrimination

Song Wang(王宋) Peng Xu(许鹏) Chang-Bing Lu(鲁昌兵)
Yong-Gang Huo(霍勇刚) Jun-Jie Zhang(张俊杰)
Xi'an Research Institute of Hi-Tech, Xi'an 710025, China

Abstract: Three algorithms (the Charge Comparison Method, n–γ Model Analysis and the Centroid Algorithm) have been revised to improve their accuracy and broaden the scope of applications to real-time digital n-γ discrimination. To evaluate the feasibility of the revised algorithms, a comparison between the improved and original versions of each is presented. To select an optimal real-time discrimination algorithm from these six algorithms (improved and original), the figure-of-merit (FOM), Peak-Threshold Ratio (PTR), Error Probability (EP) and Simulation Time (ST) for each were calculated to obtain a quantitatively comprehensive assessment of their performance. The results demonstrate that the improved algorithms have a higher accuracy, with an average improvement of 10% in FOM, 95% in PTR and 25% in EP, but all the STs are increased. Finally, the Adjustable Centroid Algorithm (ACA) is selected as the optimal algorithm for real-time digital n-γ discrimination.

Keywords: n-γ discrimination, improvement of algorithms, real-time discrimination

PACS: 29.40.-n **DOI:** 10.1088/1674-1137/40/2/026202

1 Introduction

It has been found that all neutron fields coexist with associated γ-ray backgrounds, arising as a result of reactions of the neutrons with materials in the environment and as direct byproducts of the primary reaction producing the neutron field. Therefore discriminating neutrons against a γ-ray background plays an essential role in detecting neutrons effectively [1]. Over the past few decades, various methods using analog circuit technology have been developed for n-γ discrimination, such as the Rise Time Method [2–4] and the Charge Comparison Method [5, 6]. These traditional methods always require special electronic modules, which leads to a complex system, unstable signal and higher cost.

With the development of high-speed ADC sampling technology, it is possible for the entire signal waveform to be sampled into a discrete sequence of numbers, along with which many new offline n-γ discrimination methods have been developed, such as Neural Network [7], Wavelet Transform [8] and Fuzzy Clustering [9]. These algorithms have been implemented successfully for n–γ discrimination with high accuracy. However, they are usually too complex to fulfill the requirements of real-time digital n–γ discrimination considering the current development of hardware; therefore these algorithms were excluded when selecting algorithms for real-time discrimination in our work.

Since real-time digital n-γ discrimination is urgently needed for situations such as nuclear accident emergencies, security and arms control verification, great strides have been made in real-time discrimination algorithms. These algorithms still have shortcomings, however, in their accuracy and the scope of application in different measuring conditions. Considering the performance of the traditional real-time discrimination algorithms in the time domain, the Charge Comparison Method (CCM) and n-γ Model Analysis (NGMA) [10] were selected for improvement. With its advantages in catching the features of a pulse, the Centroid Algorithm (CA) [11] was brought from the digital signal processing field to apply to real-time n-γ discrimination. The methods of improving these algorithms will be given in Section 2 and their performance will be presented in Section 3. Finally, the conclusions raised from this research will be stated in Section 4.

2 Improved algorithms

2.1 Normalized Charge Comparison Method (NCCM)

The main advantage of the Charge Comparison Method is that the stimulated light pulse contains different time delay components because of the different density of ionization ρ. The current caused by neutrons and γ-rays in a scintillator can be written as [12]:

$$I(t) = I_{\rm f}(\rho)\mathrm{e}^{-t/\tau_{\rm f}} + I_{\rm s}(\rho)\mathrm{e}^{-t/\tau_{\rm s}} \quad (1)$$

Received 20 November 2014, Revised 23 September 2015

where $\tau_{\rm f}$ and $\tau_{\rm s}$ are the time constants of the scintillator for the fast and slow components of the current, respectively; $I_{\rm f}$ and $I_{\rm s}$ are the fast and slow components of the current; and I is the total current.

The charge comparison method based on the electronics equipment can be calculated through integrating with a large time constant:

$$Q=\int_0^{\infty} I(t){\rm d}t=I_{\rm f}(\rho)\tau_{\rm f}+I_{\rm s}(\rho)\tau_{\rm s}=Q_{\rm f}(\rho)+Q_{\rm s}(\rho) \quad (2)$$

where $Q_{\rm f}$ and $Q_{\rm s}$ are the charges of the fast and slow components of the current and Q is the total change.

The $Q_{\rm f}/Q_{\rm s}$ obtained from the formula above is the discrimination factor of discriminating the n and γ-rays.

$Q_{\rm f}/Q_{\rm s}$ can be obtained from Eq. (3) for discrete pulses [5]:

$$Q_{\rm f}=\sum_{n=T_{\rm m}}^{T_{\rm s}}{\rm Pulse}(n) \quad Q_{\rm s}=\sum_{n=T_{\rm d}}^{T_{\rm s}}{\rm Pulse}(n) \quad (3)$$

where Pulse(n) is the nth point of the pulse collected with the high-speed data acquisition card, as shown in Fig.1; $T_{\rm m}$ is the pulse peak; $T_{\rm s}$ is the threshold of the stopping site, traditionally taking the first 60 channels after $T_{\rm m}$; and $T_{\rm d}$ is the time where the ratio of slow components and fast components meets its maximum value, always taking the first 15 channels after $T_{\rm m}$.

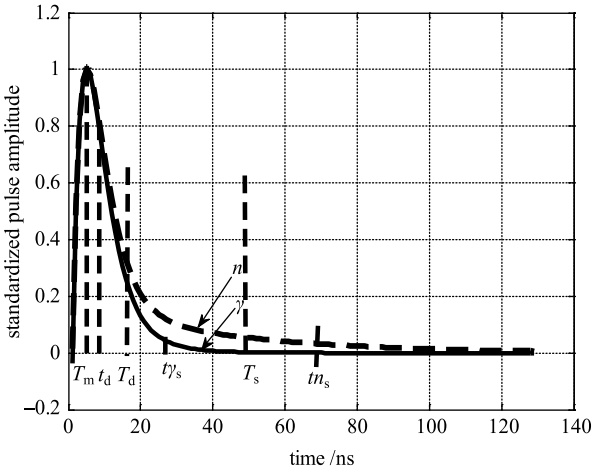

Fig. 1. Plot of normalized pulses of neutron and γ ray according to the Marrone model [15]. $T_{\rm m}$ is the pulse peak site; $T_{\rm d}$ and $T_{\rm s}$ are the lower limit and the upper limit respectively of the integral of the CCM; and $t_{\rm d}$ and $t\gamma_{\rm s}(tn_{\rm s})$ are the lower limit and the upper limit respectively of the integral of the NCCM.

When $T_{\rm s}$ and $T_{\rm d}$ are taken at fixed sites using CCM, they cannot be well suited to pulses which are collected at different sampling rates and from different source terms. Different from CCM, the NCCM uses the value of 0.03 times the maximum amplitude of the pulse as the stopping amplitude, and uses the corresponding channel site as $tn_{\rm s}$ ($t\gamma_{\rm s}$), as shown in Fig. 1. As $tn_{\rm s}$, we take the value of 0.8 times the maximum amplitude of the pulse as the corresponding amplitude of $t_{\rm d}$, where the 0.03 and 0.8 are values obtained from experiments. Then the discrimination factor G can be obtained by Eq. (4).

$$G=\frac{Q_{\rm f}}{Q_{\rm s}}=\frac{\sum\limits_{n=t_{\rm d}}^{t\gamma_{\rm s}}{\rm Pulse}(n)}{\sum\limits_{n=t_{\rm d}}^{tn_{\rm s}}{\rm Pulse}(n)} \quad (4)$$

The results show that using the vector unitization method expressed in Eq. (5) to produce these pulses before obtaining the factor G greatly benefits the effect of the discrimination [13].

$$\beta=\frac{\alpha}{\|\alpha\|}=\frac{\alpha}{\sqrt{\alpha_1^2+\alpha_2^2+\cdots+\alpha_n^2}}, \quad (5)$$

where, α is the original vector; β is the unitized vector; and α_1, α_2, $\cdots$ α_n are the elements of α.

2.2 Self-adaptive n-γ Model Analysis (ANGMA)

In NGMA, a neutron model and γ model are first given referring to Marrone's model [14], and then these models are taken to calculate $\chi_{\rm n}^2$ and χ_{γ}^2 using Eq. (7) and Eq. (8). The discrimination factor G is obtained by Eq. (9) [5].

$$x(t)=A\left[\exp\left(-\frac{t-t_0}{\theta}\right)-\exp\left(-\frac{t-t_0}{\lambda_{\rm s}}\right)+B\exp\left(-\frac{t-t_0}{\lambda_{\rm l}}\right)\right], \quad (6)$$

where $x(t)$ is the function referred to Marrone's model, that describes the pulse shapes from a scintillator detector; t is time variable; t_0 is the initial time; A and B are the amplitude of the fast and slow components respectively at $t=0$; and $\lambda_{\rm s}$ and λ_0 are the time constants of the scintillator for the fast and slow components respectively. The six parameter values for Eq. (6), for an accurate reproduction of the average neutron and γ-ray pulse shapes acquired using an EJ-301 scintillator (whose function is similar to the BC501A scintillator), are given in Ref. [14].

No optimization of parameters is required in this technique, as the unidentified digitized pulses have been compared with the modeled pulses and characterized by calculating the difference between the chi-squares for the

γ-ray model (χ^2_γ) and the neutron model ($\chi^2_{\rm n}$) using Eqs. (7)–(9).

$$\chi^2_\gamma = \sum_{i=T_{\rm m}}^{T_{\rm s}} \frac{\left(\frac{Am_\gamma}{AP_{\rm u}}P_{\rm u}(i) - m_\gamma(i)\right)^2}{m_{\rm g}(i)}, \tag{7}$$

$$\chi^2_{\rm n} = \sum_{i=T_{\rm m}}^{T_{\rm s}} \frac{\left(\frac{Am_{\rm n}}{AP_{\rm u}}P_{\rm u}(i) - m_{\rm n}(i)\right)^2}{m_{\rm n}(i)}, \tag{8}$$

where $m_{\rm g}$ is the γ model pulse; Am_γ is the area of the γ model pulse; $m_{\rm n}$ is the neutron model pulse; $Am_{\rm n}$ is the area of the neutron model pulse; $P_{\rm u}$ is the sampling pulse and $AP_{\rm u}$ is the area of sampling pulse; $T_{\rm m}$ is the time event of the pulse peak; and $T_{\rm s}$ is the time event of stopping. The stopping threshold $y_{\rm s}$ is 0.03 times the pulse peak $y_{\rm m}$.

$$G = \Delta\chi^2 = \chi^2_\gamma - \chi^2_{\rm n}. \tag{9}$$

If the pulse discrimination factor $G < 0$, the pulse is a γ-ray; otherwise it is a neutron.

NGMA is unable to adjust the length of the model pulse according to the sampling rate, the detector and the types of source terms, so it cannot be generally applied. However, ANGMA can adjust the length of its model pulse to the length of sampling pulse, and can set the peak channel and the stopping threshold channel of the model pulse according to that of the sampled standardized pulse (using Eq. (5) to standardize the sampling pulse), therefore reducing the influence of the accuracy of discrimination of different sampling rates and different sources.

2.3 Adjustable Centroid Algorithm (ACA)

The CA uses Eq. (10) to gain the "center of mass" of a curve or a signal waveform, whose concept is an "average" in statistics; the algorithm is mainly used in the digital signal processing field. Experimental results show that the CA can be implemented in the nuclear signal processing field; therefore we introduce this algorithm to nuclear signal pulse processing to discriminate neutrons and γ-rays. Theoretically, the ratio of the slow component and the fast component of the neutron pulse is greater than that of γ-rays, thus the centroid of a neutron pulse is later, while the centroid of a γ-ray pulse is further forward, and can be taken as the discrimination factor.

$$C = \frac{\sum_{n=T_{\rm m}}^{n=T_{\rm s}} n\cdot{\rm Pulse}(n)}{\sum_{n=T_{\rm m}}^{n=T_{\rm s}} {\rm Pulse}(n)} \tag{10}$$

where C is the centroid value of the pulse and Pulse (n) is the nth point from $T_{\rm m}$ of the pulse.

Figure 4 shows that the centroid changes with the pulse peak. In order to eliminate the effect of the pulse peak on the centroid, we take Eq. (11) to adjust the factor C (obtained by CA expressed in Eq. (10)), then the new ACA algorithm's discriminating factor G can be obtained [15]:

$$G = C + \begin{cases} [{\rm walk}/y_{\rm m}]^2, & 0 \leqslant {\rm walk} \leqslant y_{\rm m} \\ {\rm walk}\times y_{\rm m}, & -y_{\rm m} \leqslant {\rm walk} \leqslant 0 \end{cases} \tag{11}$$

where, $y_{\rm m}$ is a pulse peak (in order to reduce the complexity of the algorithm, $y_{\rm m}$ takes the maximum of the pulse); walk is the adjusting factor.

3 Results and discussion

The data used to test these algorithms is obtained by high-speed data acquisition card NI5772 from BC501A liquid scintillator detector provided by the Arms Control Research Office of the China Institute of Atomic Energy. The amplitude variation range of the sampling pulse is 0–5 V; the sampling rate of the ^{239}Pu and ^{252}Cf sources is 1 GHz and the sampling rate of the Am-Li source is 1.6 GHz.

3.1 Acquisition and analysis of scattering and n-γ discrimination spectrum

1) Scattering and n-γ discrimination spectrum of NCCM

Figure 2(a) and Fig. 2(b) have serious adhesion tails, which means a linear threshold is unable to be given. However, Fig. 2(d) shows that the pulses produced by the vector-unitization method can reduce the overlapping proportion of the two types of points on the x-axis, which then reduces the tail adhesions. Finally the n-γ discrimination threshold is explicitly given (shown in Fig.2 (e)). In addition, the upper and lower limits channel site of the fast and slow components of the pulse are no longer fixed; instead they are determined by the pulse amplitude, which makes the algorithm more commonly applicable. In conclusion, comparing Fig. 2(f) with Fig. 2(c), the neutron-γ discrimination spectrum obtained by NCCM significantly improves the discrimination effect over the traditional CCM method.

2) Scattering and n-γ discrimination spectrum of ANGMA

The NGMA algorithm cannot adjust itself to the pulses' own features. That is to say, when the NGMA parameters are well adjusted to produce the pulses from the ^{239}Pu source at one sampling rate, as shown in Fig. 3(a) and Fig. 3(e), these parameters cannot be well suited to pulses from the Am-Li source at another sampling rate, as shown in Fig. 3(b). That means the sampled pulse peak channels do not match those of the model,

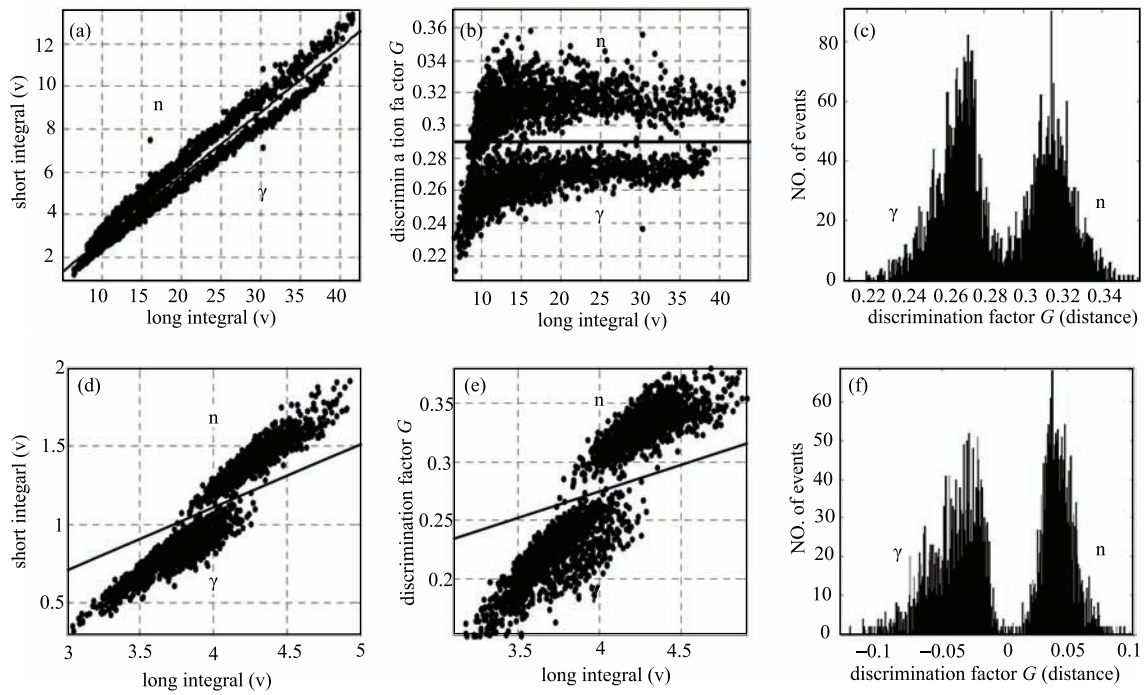

Fig. 2. CCM and NCCM discrimination with Am-Li neutron source. (a) variation of long integral varies with short integral by traditional CCM; (b) variation of G with long integration area; (c) population distribution of each point from the discrimination line; (d), (e), (f) correspond to (a), (b), (c) with NCCM.

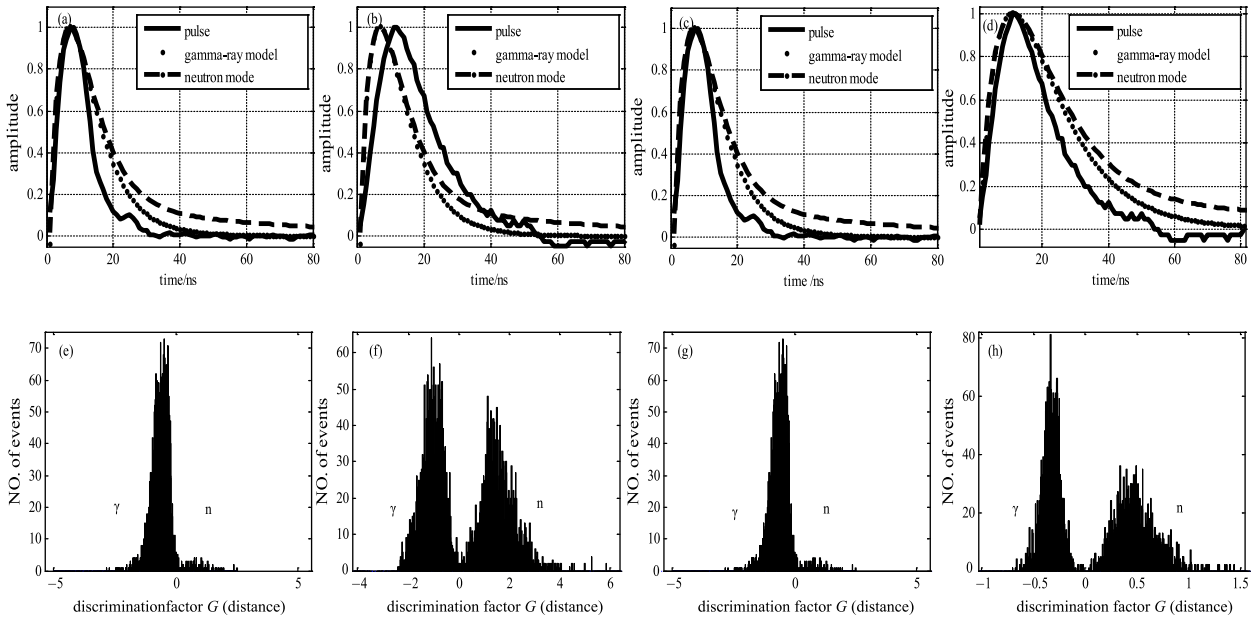

Fig. 3. Comparison between ANGMA and NGMA. (a) is the sampling pulse of ^{239}Pu source at 1 GHz sampling rate with neutron model and γ-ray model when using NGMA; (e) is the n-γ discrimination spectrum corresponding to (a); (b) is the sampling pulse of Am-Li source at 1.6 GHz sampling rate with neutron model and γ-ray model when using NGMA without parameter adjustment; (f) is the n-γ discrimination spectrum corresponding to (b); (c) is the sampling pulse of ^{239}Pu source at 1 GHz sampling rate with neutron model and γ-ray model when using ANGMA; (g) is the n-γ discrimination spectrum corresponding to (c); (d) is the sampling pulse of Am-Li source at 1.6 GHz sampling rate with neutron model and γ-ray model when using ANGMA without parameter adjustment; (h) is the n-γ discrimination spectrum corresponding to (d).

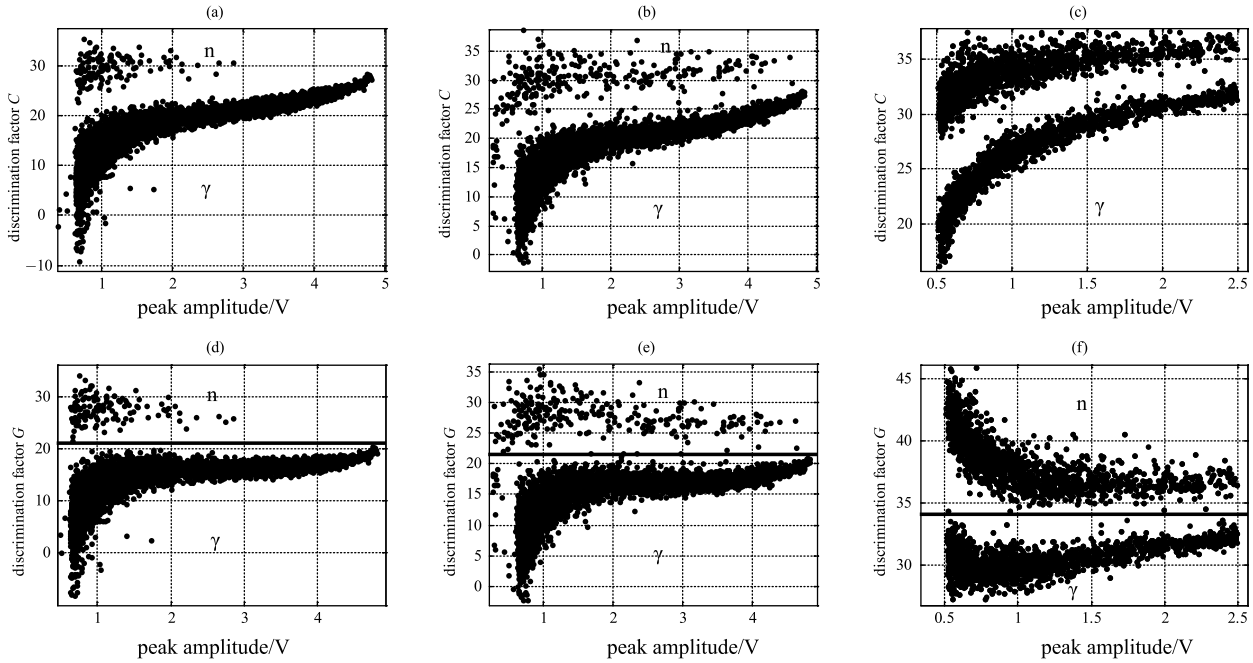

Fig. 4. Scatter diagrams of variation of G with pulse peaks, comparing CA (Centroid Algorithm) with ACA. (a)(b)(c) are respectively Pu-Li source, ^{252}Cf source and Am-Li source processed by CA; (d)(e)(f), are respectively ^{239}Pu source, ^{252}Cf source and Am-Li source processed by ACA.

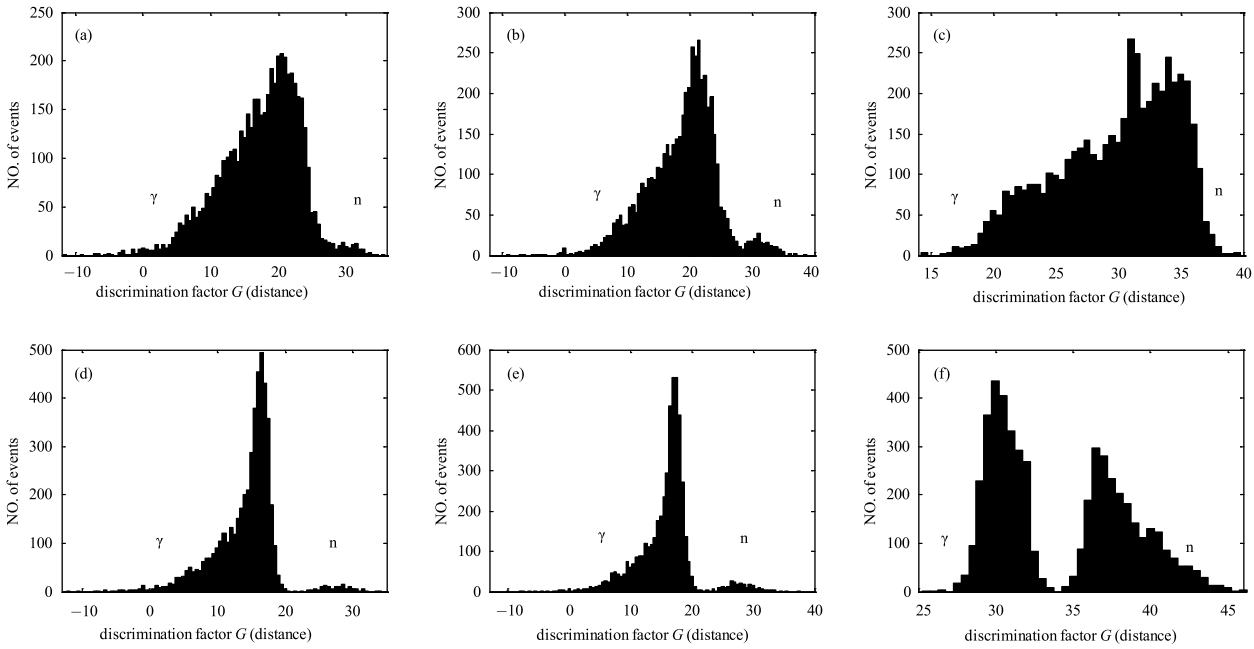

Fig. 5. Population distribution of each point from the discrimination line of CA and ACA. (a)(b)(c) are the n-γ discrimination spectra produced by CA from the ^{239}Pu source, ^{252}Cf source and Am-Li source respectively; (d)(e)(f) are the n-γ discrimination spectra produced by ACA from the ^{239}Pu source, ^{252}Cf source and Am-Li source respectively.

which leads to the n-γ particles not being easily distinguishable from the spectrum shown in Fig. 3(f). However, ANGMA can adjust itself according to the sampling pulse features, which benefits the discrimination of n-γ particles as shown in Fig. 3(d) and Fig. 3(h).

3) Scattering and n-γ discrimination spectrum of ACA

With the CA method, we obtain scatter diagrams as

shown in Fig. 4(a), (b), (c), from which neutrons and γ-rays can be separated easily by the eye. However a one-dimensional linear threshold cannot be given for the variation of the centroid with the pulse peaks, so the neutrons cannot be separated from γ-rays effectively (as shown in Fig. 5(a), (b), (c)). In order to eliminate the overlap area of the centroids at low energy with the centroids at high energy, the ACA algorithm introduces the adjusting factor 'walk'. ACA can mitigate the variation of G with pulse peak, and give a one-dimensional linear threshold, which then provides a better n-γ discrimination spectrum as shown in Fig. 5 (d), (e), (f).

3.2 Parametric analysis

To quantitatively evaluate the performance of these improved algorithms, the traditional parameters, such as number of neutrons, number of γ-rays, FOM, threshold height, threshold width, peak threshold ratio, and FOM2 obtained after Gaussian fitting are calculated in this article. In addition, the error probability in Bayesian statistics is used to conduct a comprehensive assessment of the algorithm.

To reduce the influence of randomness on the accuracy of parameters, n-γ discrimination spectra are filtered by the Butterworth window filter and phase-corrected before obtaining these parameters [16]; otherwise, the n-γ discrimination spectra are bimodal fitted by a Gaussian function [17] to get the error probability [18] and FOM2.

The parameters used are as follows:

1) Threshold (Th): The significance of the threshold obtained by Bimodal is used to judge if the channel width, the starting channel, and the cutoff channel selected to get the spectrum are reasonable.

2) Threshold height (ThH): The number of pulses corresponding to the threshold obtained.

3) Peak-to-Threshold-height Ratio (PTR): Ratio of the height of γ-ray or neutron peak (the lower one) in the n-γ discrimination spectrum to the height of the threshold as shown in Fig. 6(c),

$$\mathrm{PTR} = \frac{\text{Peak height}}{\text{Threshold height}}. \tag{12}$$

4) Threshold width (ThW): The number of channels corresponding to the half summation of the γ-ray or neutron peak (the lower one) with the threshold height in the n-γ discrimination spectrum as shown in Fig. 6(c);

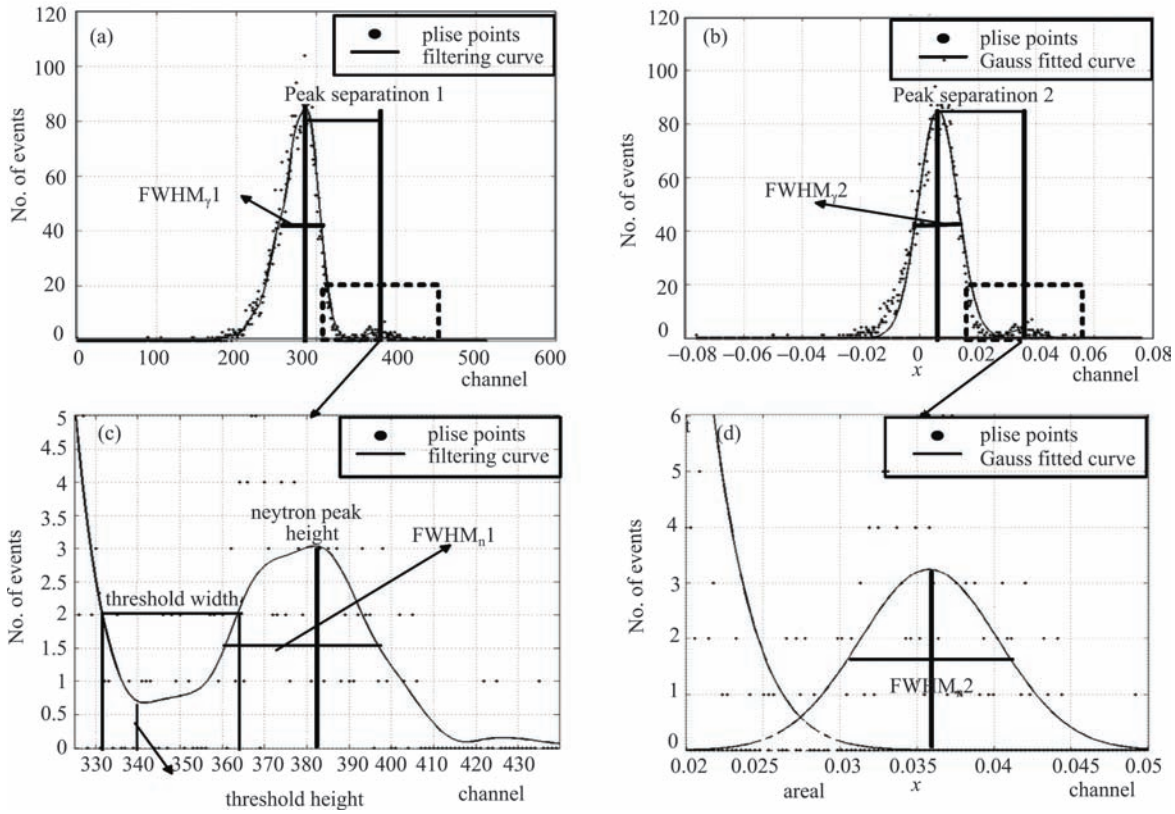

Fig. 6. Comparison of filtered and fitted n-γ discrimination spectra. (a) n-γ discrimination spectrum filtered by Butterworth window filter and phase-corrected; (c) partially enlarged view of (a); (b) n-γ discrimination spectrum bimodal fitted by Gaussian function; (d) partially enlarged view of (b). The pulses processed are from the ^{239}Pu source.

5) Figure-of-Merit1 (FOM1): The corresponding figure-of-merit1 values for each method are calculated using Eq. (13) after filtering by the Butterworth window filter and phase-correction.

$$\mathrm{FOM}=\frac{\text{Peak separation 1}}{\mathrm{FWHM1}_{\gamma}+\mathrm{FWHM1}_{\mathrm{n}}}. \tag{13}$$

6) Error Probability (EP): The minimum risk indicators in the Bayesian decision theory, calculated by Eq.(14) after fitting by a Gaussian function,

$$\mathrm{EP}=\frac{\mathrm{Are1}}{\mathrm{Are}_{\gamma}+\mathrm{Are}_{\mathrm{n}}}. \tag{14}$$

7) Figure-Of-Merit 2 (FOM2): The corresponding figure-of-merit2 values are calculated using Eq. (15) after fitting the n-γ discrimination spectrum by a Gaussian function as shown in Fig. 6(d).

$$\mathrm{FOM}=\frac{\text{Peak separation 2}}{\mathrm{FWHM2}_{\gamma}+\mathrm{FWHM2}_{\mathrm{n}}}. \tag{15}$$

8) Simulation Time (ST): ST is the time taken to simulate 5000 pulses by these algorithms with MATLAB. Although the ST for an algorithm obtained by different software and different computers is different, the result can still evaluate the performance of these algorithms with respect to their complexity.

For the entire table, ignoring the impact of noise, random effects and other factors, threshold distribution indicates the selected channel width is reasonable; and the numbers of neutrons and γ-rays calculated by the improved and original algorithms are similar, which proves that the improvement of the algorithms is reasonable.

1) Comparative analysis of NCCM and CCM. As shown in Table 1, NCCM is better than CCM with an improvement of 14.95% in FOM1, 8.67% in FOM2, 124.43% in PTR, a decrease of 29.41% in EP obtained from ^{239}Pu. For Am-Li, there is an improvement of 5.468% in FOM1, 11.57% in FOM2, 581.29% in PTR, and a decrease of 18.84% in EP. With ^{252}Cf , there is an improvement of 9.32% in FOM1 and 143.29% in PTR. However, the FOM2 and EP obtained from ^{252}Cf are inconsistent, and they may have distinctions even though the n-γ discrimination spectra have been filtered or fitted. Besides, the ST of NCCM is almost four times than that of CCM, which indicates it will take more hardware resources when applied to digital real-time n-γ discrimination.

2) Comparative analysis of ANGMA and NGMA. The sampling rate of ^{239}Pu is the same as ^{252}Cf but different to Am-Li. This paper uses pulses from ^{239}Pu and Am-Li, whose sampling rates are different, to comparatively analyze ANGMA and NGMA. The results shows that ANGMA is better than NGMA, with an improvement of 29.63% in FOM1, 19.9% in FOM2, 3745.45% in PTR, and with a decrease of 43.15% in EP. That means the parameters of NGMA adjust well to pulses from ^{239}Pu but cannot do the same for the pulses from Am-Li, while ANGMA has no problem in adjusting parameters for different rates. Therefore the ANGMA algorithm can be universally applicable, but the ST of ANGMA is 30% more than that of NGMA.

3) Comparative analysis of ACA and CA. The parameters of ^{239}Pu and Am-Li processed by CA are not given in the table, as a definite threshold cannot be obtained from their n-γ discrimination spectra. As shown in Table 1, the n-γ discrimination spectrum obtained by ACA can discriminate neutrons and γ-rays accurately, particularly for the ^{239}Pu source, whose pulses can be divided completely into two piles by ACA. The results are satisfactory, and the ST of ACA is 6% more than that of CA.

Table 1. Parameter measurements for mixed radiation fields for different neutron–γ discrimination algorithms investigated in this study.

source	algorithm	ChW	No. of n	No. of γ	Th	ThH	PTR	ThW	FOM1	EP	FOM2	ST/s
^{252}Cf	CCM	1/512	251	4749	281	2.8	2.571	17.33	0.9836	0.0024	1.067	0.151295
	NCCM	1/512	254	4746	271	0.84	6.255	37.65	1.0753	0.0076	1.022	0.572277
	CA	1/512	203	4792	307	4.35	2.040	11.76	0.7915	0.0193	0.7937	0.031432
	ACA	1/512	251	4749	276	1.0626	8.125	23.72	1.2195	0.0008	1.1933	0.034128
^{239}Pu	CCM	1/512	118	4882	329	1.27	2.960	11.13	1.0377	0.0017	1.028	0.150697
	NCCM	1/512	126	4874	346	0.513	6.643	32.82	1.1829	0.0012	1.117	0.570058
	ACA	1/512	127	4873	272	0.2125	20.604	24.73	1.3636	0.0004	1.2216	0.033378
Am-Li	CCM	1/1024	2250	2750	202	19.99	5.147	26.01	0.9692	0.0138	0.9405	0.150298
	NCCM	1/1024	2385	2615	221	1.601	35.066	40.96	1.0222	0.0112	1.0543	0.573976
	NGMA	1/1024	2395	2605	0	1.55	22.068	67.40	1.0088	0.0095	1.0283	0.561311
	ANGMA	1/1024	2408	2592	0	0.034	846.967	88.06	1.3077	0.0054	1.2329	0.782988
	ACA	1/1024	2398	2602	253	0.6217	92.409	35.47	1.4968	0.0089	1.3030	0.032521

In particular, the main improvement of the CCM algorithm is in uniting the pulses before discrimination and selecting the stopping channel based on the pulses' amplitude rather than a fixed channel. The significance of unitization is reducing the overlapping proportion of two types of points on the x-axis, thus reducing the tail adhesions. Secondly, the stopping channel is no longer fixed but refers to the pulse amplitudes to eliminate the effect of different pulse intensity on the recognition factor G. The significance of improving NGMA is to make it more universally applicable. Specifically, ANGMA performance will not deteriorate by change of sampling frequency, trigger acquisition mode, collecting length and other conditions. The significance of improving CA is to provide a one-dimensional linear threshold to discriminate neutrons and γ-rays more easily and accurately.

4 Conclusion

In this paper, three algorithms have been improved for the purpose of real-time discrimination. These improved algorithms have higher accuracy and more adaptive capability, which benefits the effectiveness of real-time n-γ discrimination. With the development of hardware technology, these improved algorithms will be applied for real-time discrimination, in spite of the increase of ST in these improved algorithms.

A comprehensive assessment obtained by comparing the original and improved algorithms indicates that ACA is the optimal algorithm for digital real-time n-γ discrimination.

We thank the Arms Control Research Office of the China Institute of Atomic Energy for providing experiment data and constructive suggestions on the standards of selecting improved algorithms.

References

1 Y. H. Chen, X. M. Chen, X. D. Zhang et al, Chin. Phys. C, **38**(3): 036001 (2014)
2 Acciarri R, Canci N, Cavanna F et al, Physics Procedia, **37**: 1113 (2012)
3 Favalli A, Iliev M L, Chung K et al, IEEE Transactions on Nuclear Science, **60**(2): 1053 (2013)
4 Y. G. Yuan, J. R. Lei, X. L. Bai, Atomic Energy Science and Technology, **44**(6): 735 (2010)(in Chinese)
5 Sderström P A, Nyberg J, Wolters R, arXiv:0805.0692v1 (2008 May 6)
6 Gamage A A K, Joyce J M, Hawkes P N, Nuclear Instruments and Methods in Physics Research A, **642:** 78–83 (2011)
7 L. Zhang, *Analysis and Optimization of Several Neural Networks and Their Applications*, PH.D Thesis (Xi'an: Electron University of Science and Technology, 2012) (in Chinese)
8 X. Li, *Studies of Underwater Signal Processing Based on Continuous Wavelet Transform*, PH.D Thesis (Xi'an, Northwestern Polytechnical University, 2003) (in Chinese)
9 X. L. Luo, *Research on the n/γ Discrimination Method Based on Fuzzy Cluster Analysis M.S. Thesis* (School of National University of Defense Technology, 2010) (in Chinese)
10 Valdemar Rørbech, *Processing and classification of hydroacoustic signals for nuclear test-ban-treaty verification*, M.S. Thesis (University of Copenhagen, 2011)
11 X. L. Luo, G. F. Liu, J. Yang et al, Atomic Energy Science and Technology, **47**(8): 1405 (2013)(in Chinese)
12 Y. Chen, Z. J. Wang, High Energy Physics and Nuclear Physics, **23**(7): 616 (1999)
13 E. F. Wang, *Linear Algebra* (Beijing: Tsinghua University Press, 2007)
14 MARRONE S, CANO-OTT D, COLONNA N et al, Nuclear Instruments and Methods in Physics Research A, **490**(5): 299 (2002)
15 Andreas Ruben, Timothy E et al, MPD4-NSS-MIC07_N15-273
16 P. X. Cheng, *Digital Signal Processing* (Beijing: Tsinghua University Press, 2007)
17 Chris Wyman, Journal of Computer Graphics Techniques, **2**(2): http://jcgt.org, 2013
18 B. X. Li, *Principles and Applications of Pattern Recognition* (Xi'an: Electron University of Science and Technology Press, 2008)